Mobility of surface species on oxides. 1 Isotopic exchange of 18O2 with 16O of SiO2, Al2O3, ZrO2, MgO, CeO2, and CeO2−Al2O3. Activation by noble metals. Correlation with oxide basi...

ARTICLE *in* THE JOURNAL OF PHYSICAL CHEMISTRY · MAY 1996

Impact Factor: 2.78 · DOI: 10.1021/jp9531568

Mobility of Surface Species on Oxides. 1. Isotopic Exchange of $^{18}O_2$ with ^{16}O of SiO_2, Al_2O_3, ZrO_2, MgO, CeO_2, and CeO_2-Al_2O_3. Activation by Noble Metals. Correlation with Oxide Basicity†

Dominique Martin and Daniel Duprez*

Laboratoire de Catalyse en Chimie Organique, 40 Av. du Recteur Pineau, 86022 Poitiers Cedex, France

Received: October 26, 1995; In Final Form: February 13, 1996[⊗]

Temperature-programmed isotopic exchange of $^{18}O_2$ with ^{16}O of several oxides was carried out in the 200−900 °C temperature range. The oxides can be ranked according to their maximal rates of exchange obtained at the following temperatures: CeO_2, 410 °C ≫ CeO_2-Al_2O_3, 480 °C ≈ MgO, 490 °C > ZrO_2, 530 °C ≫ γ-Al_2O_3, 620 °C ≫ SiO_2, 850 °C. Except on CeO_2 and on CeO_2-Al_2O_3 a simple exchange yielding initially $^{18}O^{16}O$ can be observed. With ceria containing oxides, the reaction occurs in part via a multiple exchange mechanism yielding initially $^{16}O_2$ which is indicative of the presence of binuclear species (O_2, O_2^-, or O_2^{2-}) at the ceria surface. Chlorine-free rhodium catalysts supported on these oxides were prepared with metal dispersions between 32 and 89%. The presence of rhodium accelerates considerably the oxygen exchange with the support: the maximal rates of the exchange can be observed at much lower temperatures, by about 200−300 °C with respect to the bare oxides. This is attributed to a spillover of oxygen from the rhodium particles to the support. Isotopic exchange experiments carried out at temperatures (300−400 °C) at which the direct exchange is negligible allow for calculation of the coefficient of surface diffusion of oxygen on the oxides. At 400 °C, the relative mobility of oxygen (base 100 for γ-Al_2O_3) is CeO_2, 28 100 ≫ MgO, 500 > ZrO_2, 280 > CeO_2-Al_2O_3, 180 > γ-Al_2O_3, 100 ≫ SiO_2, 1.7. Oxygen mobility can be paralleled with the surface concentration of basic sites measured by CO_2 chemisorption (sites per nm^{-2}): CeO_2, 3.23 > MgO, 1.77 > ZrO_2, 1.45 > CeO_2-Al_2O_3, 0.44 > γ-Al_2O_3, 0.17 > SiO_2, ≈ 0. Actually, the basicity of CeO_2 cannot alone explain the exceptional mobility of oxygen on this oxide, due to a large part to the presence of oxygen vacancies. Above 400 °C, bulk oxygen diffusion can be observed on CeO_2, ZrO_2, γ-Al_2O_3 and CeO_2-Al_2O_3. Ceria possesses a very high internal mobility. The coefficient of bulk diffusion of oxygen in ZrO_2 is about two orders of magnitude higher than in γ-Al_2O_3, which contrasts with the relatively close values of their surface mobility. Except for CeO_2, there is a good correlation between this surface mobility and the metal−oxygen bond strength in the oxide crystal.

1. Introduction

Surface mobility phenomena of active species play an important role in catalysis, not only in the catalytic process itself but also during activation or regeneration treatments of the catalysts. Steam reforming of hydrocarbons,[1−3] oxygen storage capacity in three-way catalysts,[4] and remote control effect during selective oxidations[5] as well as any reactions involving spillover of active species[6−11] are well-known examples where the migration of surface species can play a determining role in catalysis.

These mobility phenomena have been invoked by many authors and considered as an elementary step of mechanisms of reaction, but their influences on the kinetic of reactions have been rarely discussed because very few data existed concerning the mobility of oxygen and hydrogen species.

The aim of this series of papers is to study and to compare the mobility of oxygen (Part 1) and of hydrogen (Part 2) species on the surface of several oxides chosen for reason of their use as carriers in metal catalysis. The activation of mobility phenomena caused by noble metals will also be described. In this first part, by means of isotopic exchange of $^{18}O_{2\ (gas)}$ with $^{16}O_{\ (sup.)}$, we shall study oxygen mobility first on bare oxides and then on metal catalysts supported on these oxides. The experiments carried out on bare oxides are similar in principle to those previously reported by Winter,[12,13] Boreskov,[14,15] and Novakova.[16,17] However, in this case, temperature-programmed isotopic exchange (TPIE) instead of isothermal isotopic exchange (ISIE) was preferred so as to obtain rapidly an indication of the temperature at which the oxide exchanges oxygen. The role of metal particles is to act as an oxygen porthole on the support. It has been proven that under certain conditions, coefficient of surface diffusion can be deduced from ISIE experiments.[18]

Oxygen mobility can be linked to a $O^{2-}-M^{n+}$ bond at the oxide surface and thus to the number and the strength of the basic sites at the surface of the solid. Therefore a correlation between the oxygen mobility and the surface basicity has been tentatively verified. The use of probe molecules for the characterization of oxide surface basicity is a well-adapted test.[19] Carbon dioxide, because of its acidity and of the large number of adsorbed species formed is often used [19−22] as the probe molecule to measure surface basicity in numerous oxides. CO_2 chemisorption was thus chosen to measure oxide basicity and to try to establish a correlation between surface basicity and oxygen surface mobility.

2. Experimental Section

2.1. Materials. We used in TPIE experiments five oxides supplied by different firms: SiO_2 (Aerosil D200, Degussa),

† Keywords: oxygen isotopic exchange on alumina, ceria, magnesia, zirconia, silica; oxygen spillover; surface diffusion coefficients, correlation with surface basicity.

* To whom correspondence should be addressed.

⊗ Abstract published in *Advance ACS Abstracts,* May 1, 1996.

S0022-3654(95)03156-X CCC: $12.00

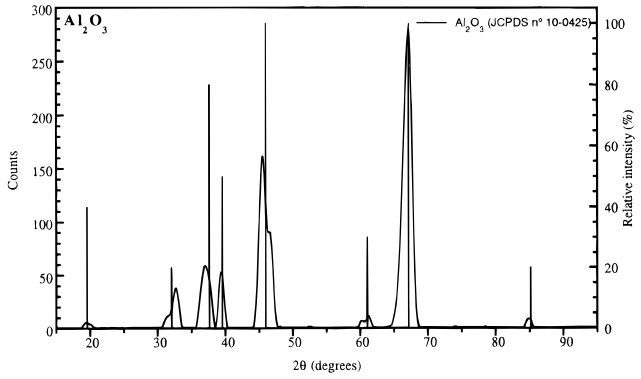

Figure 1. XRD pattern of Al_2O_3 identified as a γ alumina by comparison with JCPDS file n° 10-0425.

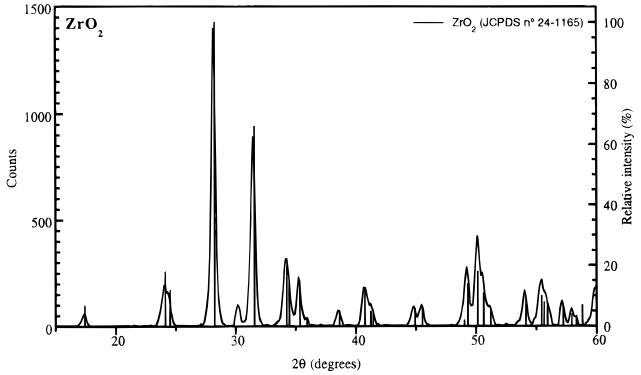

Figure 2. XRD pattern of ZrO_2 identified as a monoclinic zirconia by comparison with JCPDS file n° 24-1165.

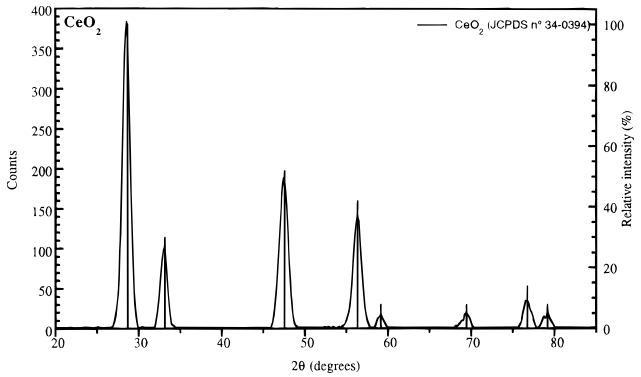

Figure 3. XRD pattern of CeO_2 identified as a cubic ceria (fluorite structure) by comparison with JCPDS file n° 34-394.

Al_2O_3 (E1633, Institut Français du Pétrole), ZrO_2 (Zirkonoxid, Degussa), MgO (100A, Ube), CeO_2 (HSA, Rhône Poulenc), and one modified oxide CeO_2-Al_2O_3 prepared by impregnation of alumina with an aqueous solution of hexanitrodiammine cerium (IV). All the oxides were crushed and sieved to 0.1−0.2 mm and calcined in air at 450 °C for 4 h.

The crystalline oxide structures were determined by X-ray powder diffraction (D500 Siemens). These measurements allow us to identify the structure of each oxide by comparison with JCPDS files. While SiO_2 is an amorphous silica, Al_2O_3 is found as a γ alumina (JCPDS file n° 10-0425, Figure 1), ZrO_2 as a pure monoclinic ("baddeleyite") zirconia (JCPDS file n° 24-1165, Figure 2), and CeO_2 as a pure cubic (fluorite type) ceria (JCPDS file n° 34-0394, Figure 3). As for MgO (Figure 4), two structures were identified, one corresponding to a cubic magnesia (JCPDS file n° 07-0239) and the other to magnesium hydroxide (JCPDS file n° 04-0823). XRD measurements of the modified CeO_2-Al_2O_3 oxide (Figure 5) show that two separate oxide phases are detected corresponding to ceria and alumina. No diffraction peak corresponding to $CeAlO_3$ oxide

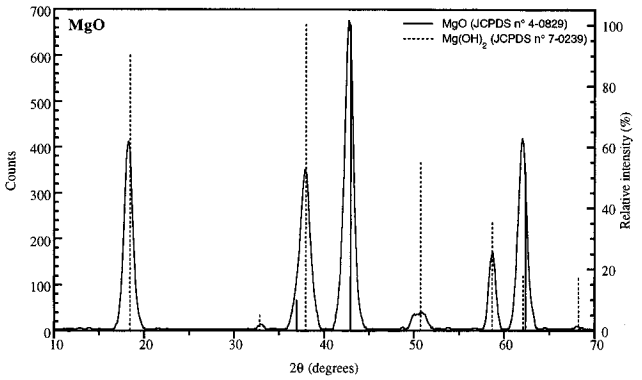

Figure 4. XRD pattern of MgO identified as a cubic magnesia (JCPDS file n° 07-0239) containing a magnesium hydroxide phase (JCPDS file n° 04-0823).

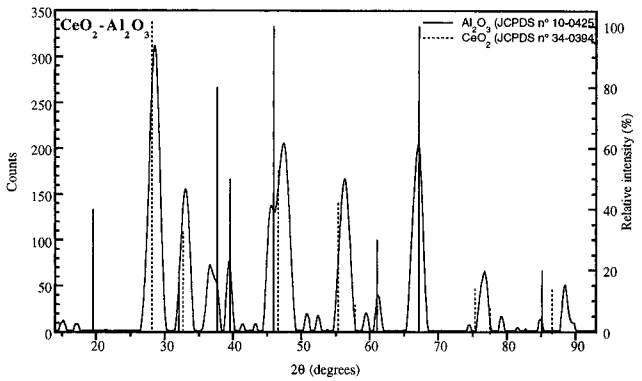

Figure 5. XRD pattern of CeO_2-Al_2O_3 identified a mixture of a gamma alumina phase (JCPDS file n° 10-0425) and a cubic ceria phase (JCPDS file n° 34-394).

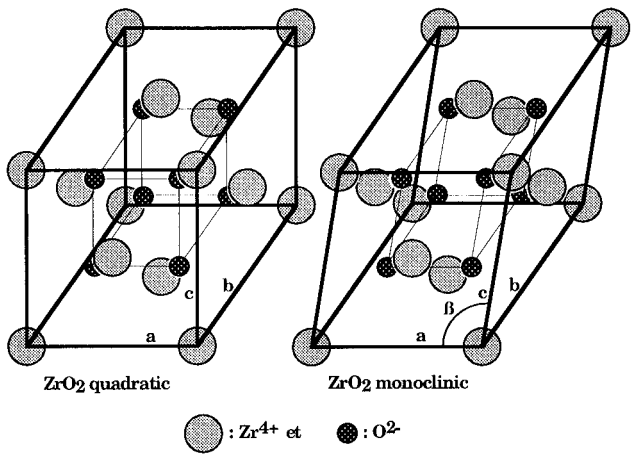

Figure 6. Comparison of the quadratic and the monoclinic zirconia structure (idealized).

was found: this cerium III aluminate can only be formed at elevated temperature in reducing environment,[23,24] most often in the presence of a noble metal.[25] However the formation of a solid solution of Ce ions in the γ-Al_2O_3 structure cannot be excluded:[26] in this case, some octahedral positions of the spinel structure would be occupied by Ce ions. With zirconium oxide, it is to be noted that the monoclinic structure is derived from a quadratic structure (Figure 6). In fact quadratic zirconia is stable even if the crystallite size is under 300 Å.[27] During calcination the crystallites reach this critical size at 850 °C, and the predominant structure is then monoclinic.[28] This structure transition provokes a significant modification of the coordination of Zr. Owing to the lattice deformation, Zr is octa-coordinated to oxygen in the quadratic structure, even though the zirconium is hepta-coordinated in the monoclinic structure.[29] In this case

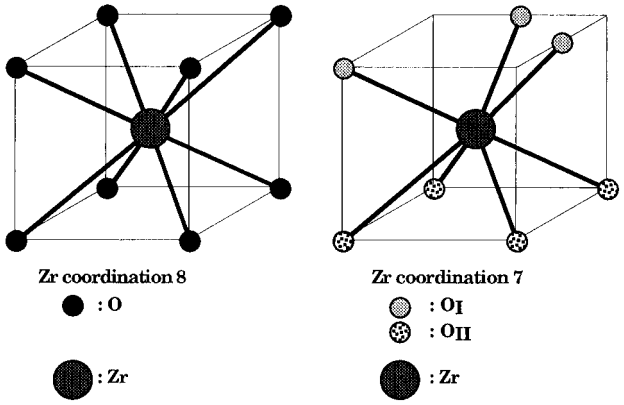

Figure 7. Zirconium coordination in the quadratic and in the monoclinic structures (idealized).

TABLE 1: Nomenclature and Characteristics of the Oxides and the Catalysts

oxide	principal impurities (ppm)	BET area ($m^2\ g^{-1}$)	catalyst name	metal loading (%wt)	N_{metal} (μmol g^{-1})	metal dispersion (%)
SiO_2	Al : 500 Ti : 300 Cl : 250	200	RhSi	Rh : 0.6	58.3	38
γ-Al_2O_3	Na : 460 Ca : 560 Si : 310 Cl : 80	100	RhAl	Rh : 0.5	48.5	87
ZrO_2	Al : 2000 Si : 100	40	RhZr	Rh : 0.6	58.3	66
	Ti : 100 Cl : 1000		PtZr	Pt : 1.2	61.5	24
MgO	Si : 20 Ca : 20	150	RhMg	Rh : 0.5	48.5	46
CeO_2	La :1500	60	RhCe	Rh : 0.6	58.3	32
CeO_2-Al_2O_3	Na : 460 Ca : 560 Si : 310 Cl : 80	100	RhCeAl	Rh : 0.5	48.5	89

(Figure 7), there are two different types of oxygen. The O_I is coordinated to three Zr atoms in a configuration approximately planar. The O_{II} is tetra-coordinated in a distorted tetrahedral configuration. The parameters of this baddeleyite zirconia structure first determined by McCullough and Trueblood[29] and specified by Smith and Newkirk[30] are $a = 5.145$ Å, $b = 5.207$ Å, $c = 5.311$ Å, and $\beta = 99.23°$ Å, with a Zr−O bond distance of 2.05 to 2.28 Å.

On these carriers, metal supported catalysts were prepared by impregnation with aqueous solutions of rhodium(III) nitrate and of dinitrodiamine platinum(II). We chose a chlorine free metal salt precursor because oxygen exchange was found to be strongly inhibited by chloride ions.[31] After impregnation, the catalysts were dried overnight at 120 °C and calcined for 4 h in air at 450 °C. Table 1 gives the nomenclature and the characteristics of oxides and catalysts used. Dispersion measurements were carried out on reduced catalysts (H_2, 450 °C) in a pulse chromatographic system previously described.[32] For the ceria free samples, metal dispersion was deduced from oxygen titration of the chemisorbed hydrogen using the following stoichiometries: $H/Rh_s = 1$, $O/Rh_s = 1.5$ and $H/Pt_s = 1$, $O/Pt_s = 1$ (see Table 1). On ceria containing catalysts, only hydrogen chemisorption can be used to determine metal dispersion because oxygen can titrate the reduced sites of ceria formed during the pretreatment.[33]

2.2. Isotopic Exchange Experiments. The isotopic exchange experiments were carried out in a recycle micro reactor (ca. 50 cm^3) coupled to a mass spectrometer (QMG Balzers). The masses 32, 34, 36 (for oxygen isotopomers[59]) plus mass 28 (to detect a possible leak) (Figure 8) were monitored every

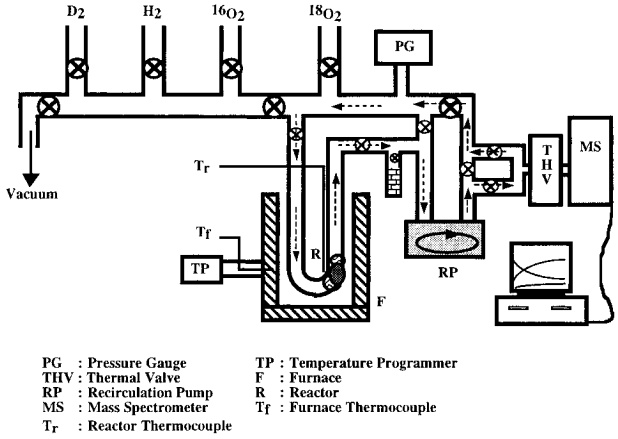

Figure 8. Isotopic exchange apparatus.

9 s. The vacuum connection to the mass spectrometer was thermoregulated so as to maintain a constant pressure of 10^{-6} mbar in the ionization chamber, while the total pressure in the reactor was 40 mbar for ISIE and 100 mbar for TPIE experiments. Under these conditions, the vacuum connection creates a negligible decrease of the total microreactor pressure (2 mbar for 2 h for an initial pressure of 40 mbar). Moreover no gas phase limiting diffusion was observed.

For TPIE, the oxide samples (5 m^2) inserted in a quartz reactor was submitted to an "in-situ" standard pretreatment. After an oxidation by normal oxygen during 15 min at 450 °C, a reduction under hydrogen during 15 min at 450 °C and an outgassing at 450 °C for 30 min, the sample was cooled down to room temperature under vacuum. A 100 mbar dose of pure $^{18}O_2$ (98,6% of ^{18}O, Isotec) was then introduced into the reactor, and the temperature increased from 25 °C to 800 °C at 2 °C min^{-1}. The pressure variation of the oxygen isotopomers P_{36} ($^{18}O_2$), P_{34} ($^{18}O^{16}O$), and P_{32} ($^{16}O_2$) were then recorded every nine seconds. The total pressure ($P_{36} + P_{34} + P_{32}$) remained virtually constant.

For ISIE, the metal catalyst samples (10−50 mg) underwent the same "in-situ" standard pretreatment as above and a 40 mbar dose of pure $^{18}O_2$ or an equimolecular mixture of $^{18}O_2$ and of $^{16}O_2$ were introduced at the exchange temperature (250−450 °C). The pressure variations of the oxygen isotopomers were then recorded every 9 s for 2 h at the temperature of reaction.

2.3. CO_2 Chemisorption. CO_2 chemisorption measurements were carried out on calcined bare oxide in a pulse chromatographic system previously described.[32] The oxide sample (0.1 g) was first flushed with He for 0.25 h at 500 °C and cooled down to room temperature. Pulses of CO_2 (0.26 cm^3) were injected into a He flow every 3 min till saturation. Following this chemisorption, the amount of CO_2 desorbed between 25 and 500 °C (23 °C min^{-1}) was measured. After cooling the reactor down to room temperature under a He flow, a second chemisorption was carried out following the same procedure.

3. Isotopic Exchange: Mechanisms and Kinetic Equations

3.1. Isotopic Exchange Mechanisms. According to Boreskov[14,15] and Novakova[16,17] three types of exchange, described by the following eqs, could occur on oxide surfaces.

(**a**) The homoexchange (or equilibration) that occurs without appreciable participation of the oxygen of the oxide (1)

$$^{18}O_{2(gas)} + {}^{16}O_{2(gas)} \rightleftharpoons 2\,{}^{18}O^{16}O_{(gas)} \qquad (1)$$

This reaction occurs according to a mechanism of adsorption−desorption. The rate of exchange of the oxygen surface species

of the oxide is negligible. During this homoexchange, the isotopic oxygen fraction in the gas phase remains constant.

(**b**) The simple heteroexchange that occurs with the participation of only one oxygen of the oxide at each step of the following eq 2

$$^{18}O^{18}O_{(gas)} + {}^{16}O_{(sup.)} \rightleftharpoons {}^{18}O^{16}O_{(gas)} + {}^{18}O_{(sup.)}$$

$$^{18}O^{16}O_{(gas)} + {}^{16}O_{(sup.)} \rightleftharpoons {}^{16}O^{16}O_{(gas)} + {}^{18}O_{(sup.)} \quad (2)$$

During this simple heteroexchange on oxide surfaces, the formation of a triatomic surface intermediate $(O_3)^-_{ads.}$ has been envisaged.[34−36]

(**c**) The multiple heteroexchange, that occurs with the participation of two oxygen atoms of the oxide at each step of the following eq 3

$$^{18}O^{18}O_{(gas)} + 2{}^{16}O_{(sup.)} \rightleftharpoons {}^{16}O_{2(gas)} + 2{}^{18}O_{(sup.)}$$

$$^{18}O^{16}O_{(gas)} + 2{}^{16}O_{(sup.)} \rightleftharpoons {}^{16}O_{2(gas)} + {}^{16}O_{(sup.)} + {}^{18}O_{(sup.)} \quad (3)$$

$$^{18}O^{16}O_{(gas)} + 2{}^{18}O_{(sup.)} \rightleftharpoons {}^{18}O_{2(gas)} + {}^{16}O_{(sup.)} + {}^{18}O_{(sup.)}$$

For this multiple exchange on oxide surfaces, there are two possible mechanisms: isotopic exchange and "place-exchange". These two mechanisms differ by the oxygen surface intermediates involved. Isotopic exchange mechanism occurs through an associative mechanism with a four-atomic $(O_4)^-_{ads.}$ surface intermediate.[36,37] On the contrary, "place-exchange" mechanism occurs without requiring a four-atom oxygen intermediate on the surface: there is just a displacement of a preadsorbed molecule by a gas phase molecule.[36,38] This mechanism does not involve the scission of any O−O bond.

TPIE experiments carried out on oxides allow us to determine the temperature range and the rate of exchange as well as the type of mechanism involved on each oxide and the number of oxygen atoms exchanged. On metal supported catalysts, ISIE experiments occur following the simple heteroexchange (**b**), the metal particles acting as donors of monoatomic oxygen species. In this case, under certain conditions, the coefficients of surface and of bulk oxygen diffusion could be measured. The eqs used to determine these parameters are the following.

3.2. TPIE Experiments. Rate of Exchange. From the partial pressure values, we can first define the oxygen 18 atomic fraction in gas phase at each time, α_g^t, as

$$\alpha_g^t = \frac{\frac{1}{2}\cdot P_{34}^t + P_{36}^t}{P_{36}^t + P_{34}^t + P_{32}^t} \quad (4)$$

The rate of exchange R_e being equal to the rate of disappearance of ^{18}O from the gas phase, it was possible therefore to determine R_e by eq 5

$$R_e = -N_g\cdot\frac{d\alpha_g^t}{dt} = N_s\cdot\frac{d\alpha_s^t}{dt} \quad (5)$$

where N_g and N_s are respectively the total number of oxygen atoms in gas phase and the number of exchangeable oxygen atoms at the oxide surface.

So R_e (in atoms per square meter and per time unit) can be obtained by eq 6

$$R_e = -\frac{N_A\cdot P_T}{S\cdot R}\cdot\left(\frac{V_r}{T_r} + \frac{V_c}{T_c}\right)\cdot\frac{d\alpha_g^t}{dt} \quad (6)$$

where N_A is the Avogadro number, P_T the total pressure, S the oxide BET area (m^2), R the gas constant, V_r and V_c respectively the volumes of the heated and unheated zone of the reactor, and T_r and T_c respectively the temperatures of the heated and unheated zone of the reactor.

Number of Exchanged Oxygen. The number of oxygen atoms exchanged at each time N_e^t is given by eq 7 at each temperature

$$N_e^t = (\alpha_g^o - \alpha_g^t)\cdot N_g \quad (7)$$

where: α_g^o is the initial atomic fraction of isotopic oxygen in gas phase.

3.3. ISIE Experiments. Rate of Exchange and Number of Exchangeable Oxygen Atoms. For ISIE experiments on metal supported catalysts, the exchange occurs through metal particles which catalyze the dissociative adsorption of gas phase oxygen molecules. Under these conditions, we showed in a previous paper[39] that the initial rate of oxygen exchange R_e^o and the number of exchangeable oxygen atoms N_s could be found by the following eqs:

$$R_e^o = -\frac{N_A}{S\cdot R}\cdot\left(\frac{V_r}{T_r} + \frac{V_c}{T_c}\right)\cdot\left(2\cdot\frac{dP_{36}^o}{dt} + \frac{dP_{34}^o}{dt}\right) \quad (8)$$

$$N_s = \frac{\alpha_g^o - \alpha^*}{\alpha^* - \alpha_s^o}\cdot N_g \quad (9)$$

where

$$\frac{dP_{36}^o}{dt} \quad \text{and} \quad \frac{dP_{34}^o}{dt}$$

are the initial slopes of the partial pressures of $^{18}O_2$ and $^{16}O^{18}O$, α_s^o is the natural isotopic abundance of ^{18}O atoms in the oxide, and α^* is the atomic fraction of ^{18}O at equilibrium in gas phase.

Coefficients of Oxygen Surface and Bulk Diffusion. When the surface migration is the rate determining step of oxygen migration, the rate of exchange depends both upon the coefficient of surface diffusion D_s and the specific perimeter I_o of the particles considered as circular sources of oxygen atom species. In this model, previously used by Kramer and Andre,[40] Cavanagh and Yates,[41] and Duprez and Miloudi,[42] the number of atoms diffused N_e^t at the beginning of exchange would amount to:

$$N_e^t = 4NrC_{^{18}O}\sqrt{\pi D_s t} \quad \text{with} \quad I_o = N\cdot(2\pi r) \quad (10)$$

where $C_{^{18}O}$, r, and I_o are, respectively, the concentration of isotopic oxygen, the radius, and the circumference of the metal particles (N particles per m^2). This model is only valid if the concentration of ^{18}O on the metal particles remains constant during the experiment. So in the case of isotopic exchange, this model could only be used at the start of exchange when $C_{^{18}O}$ is equal to the surface concentration of oxygen on metal surface particles. Under these conditions, the coefficient of surface diffusion could be calculated by the following formula 11

$$D_s = \left(\frac{\pi}{4}\right)\cdot\left(\frac{S_1}{C^*_X\cdot I_o}\right)^2 \quad \text{with} \quad S_1 = \frac{dN_e^t}{d\sqrt{t}} \quad (11)$$

where S_1 is the initial slope of the curve representing the variation of N_e^t as a function of $\sqrt{t}$ (see Figure 9).

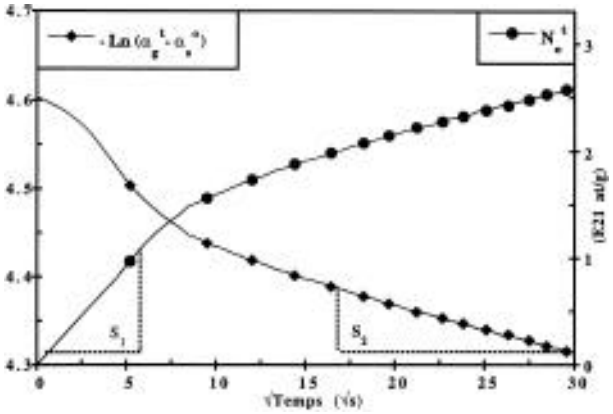

Figure 9. Curves allowing the calculation of the coefficients of diffusion.

Moreover, if a bulk oxygen diffusion phenomenon occurs, we can then determine also a coefficient of oxygen bulk diffusion D_b according to the model of Kakioka et al.[43] which leads to eq 12

$$\ln(\alpha_g^t - \alpha_s^o) = -\frac{\rho S}{N_g}\cdot\sqrt{\frac{4D_b}{\pi}}\cdot\sqrt{t} + \ln(\alpha^* - \alpha_s^o) \quad (12)$$

where ρ and S are, respectively, the density and the surface of the sample used, N_g is the total amount of oxygen atoms in gas phase, and α_g^t, α_s^o; α^* are, respectively, the atomic fractions of oxygen 18 at time t in gas phase, at time $t = 0$ in solid phase, and at equilibrium.

The measurement of the final slope S_2 (when surface has reached exchange equilibrium) of the curve representing $-\ln \alpha_g^t - \alpha_s^o$ versus $\sqrt{t}$ (see Figure 9) allows us to determine the coefficient of bulk oxygen diffusion (13)

$$D_b = \left(\frac{\pi}{4}\right)\cdot\left(\frac{S_2\cdot N_g}{\rho\cdot S}\right)^2 \quad (13)$$

Rate of Equilibration. To determine the temperature range where the rate of the adsorption−desorption step of oxygen on metal particles is not the rate determine step (RDS) of the exchange reaction, we must carry out equilibration reactions on metal catalysts, that differ from exchange reactions by the composition of the initial gas phase (compare eqs 1 and 2). During equilibration reactions, the initial gas phase is composed of an equimolecular mixture of $^{16}O_2$ and $^{18}O_2$. We can then determine from these experiments the initial rate of oxygen adsorption−desorption on metal particles R_{eq}^o with eq 14

$$R_{eq}^o = -\frac{N_A}{S\cdot R}\cdot\left(\frac{V_r}{T_r} + \frac{V_c}{T_c}\right)\cdot\frac{dP_{34}^o}{dt} \quad (14)$$

Comparison between the activation energies of exchange and equilibration reactions within a large range of temperature allows us to determine the temperature range in which we can measure surface mobility (see section 4.2.2.).

4. Results

4.1. Isotopic Exchange on Oxides. 4.1.1. Exchange Mechanism. The variation of the partial pressures of the different isotopomers of oxygen during the exchange is an indication of the principal scheme of exchange (simple or multiple, see eqs 2 and 3).

The faster increase of P_{34} than of P_{32} at the beginning of the exchange (Figure 10) on silica, alumina, zirconia, and magnesia

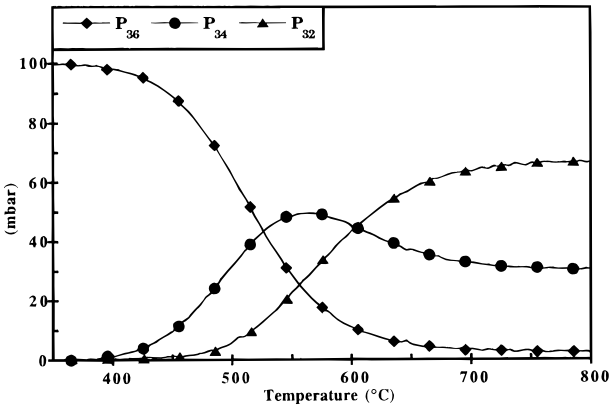

Figure 10. Variations of the partial pressures of the oxygen isotopomers during TPIE on zirconia.

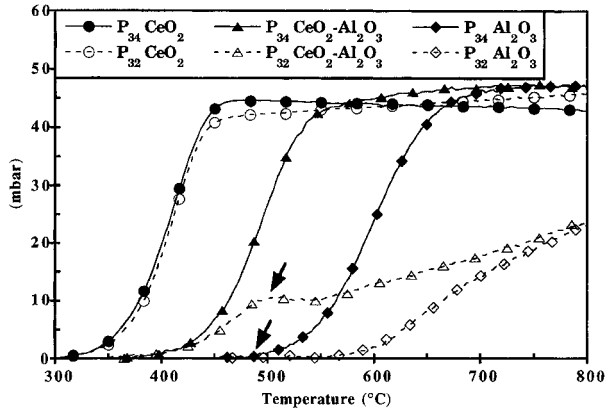

Figure 11. Comparison of the partial pressures of the oxygen isotopomer products during TPIE experiments on ceria, ceria-alumina, and alumina.

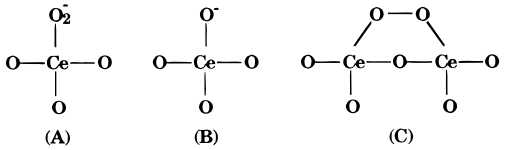

Figure 12. Surface oxygen species existing on ceria during oxygen storage, according to Yao et al.[4]

indicates that the simple exchange mechanism is favored on these oxides.

On ceria (Figure 11) oxygen is exchanged at the same proportion by simple and multiple exchange mechanisms. During TPIE experiments on ceria preoxidized samples, Cunningham et al.[44] observed only a multiple exchange mechanism between $^{16}O_2$ and $^{18}O_2$ without any trace of $^{16}O^{18}O$ product in the temperature range of 450−650 °C. For this exchange, the authors suggested a "place-exchange" mechanism. In our work the isotopic exchange starts at 310 °C. It consists of a simple and a multiple exchange mechanisms (Figure 11) which implies there are oxygen anion vacancies in the CeO_2 fluorite structure, promoting both types of exchange by decreasing the threshold temperature. The adsorption of oxygen on prereduced ceria samples almost leads to a reoxidation at room temperature.[33] It seems that this reoxidation which can occur here with the oxygen used to study the exchange proceeds with very mobile oxygen species and leads to an excess of oxygen uptake due in particular to the existence of different oxygen species (mono- and diatomic). Theses species could be superoxides (O_2^-) and peroxides (O_2^{2-}) (Figure 12) as proposed by Yao and Yao,[4] and shown by EPR for superoxides[45,46] and by FTIR in the case of peroxide species observed after oxygen adsorption on a partially prereduced ceria sample.[47] Recently, ISIE experiments

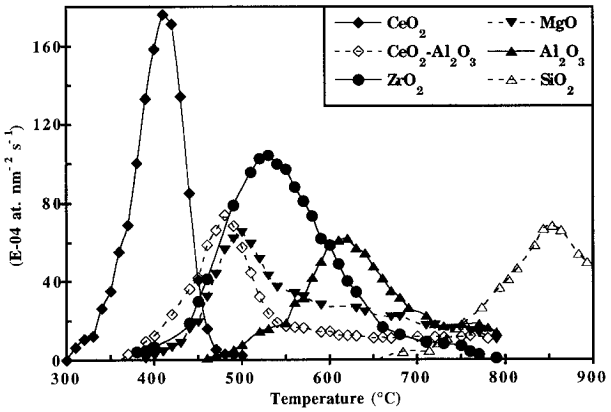

Figure 13. Rates of TPIE of oxygen on oxides.

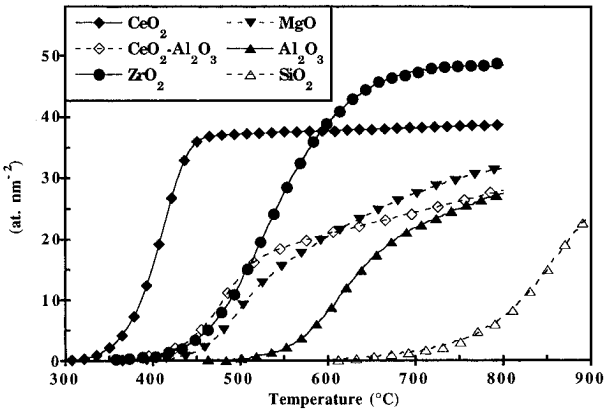

Figure 14. Number of oxygen species exchanged during TPIE of oxygen on oxides.

carried out on ceria prereduced or oxidized samples confirmed the presence of surface diatomic species which are very mobile and very sensitive to pretreatment conditions.[48]

The simple exchange is the principal mechanism on alumina whereas on ceria both simple and multiple exchanges occur in the same proportion, the behavior of ceria-alumina oxide is more complicated (Figure 11). On this modified oxide, in the 370−490 °C temperature range, where alumina alone is not exchanged the mechanism corresponds to both simple and multiple exchanges like on ceria oxide. This observation indicates that within this temperature range exchange occurs only through ceria oxide supported at the alumina surface. When the temperature is below 490 °C, alumina alone is able to exchange, and the variations of the partial pressures of oxygen isotopomers on ceria-alumina oxide indicate that the simple exchange is the principal mechanism in this temperature range. This biphasic oxide does not exchange like a simple mechanical mixture of ceria and alumina that would lead to two peaks of exchange. Even if no mixed oxide structure like $CeAlO_3$ was detected by XRD. There are strong interactions between ceria and alumina. The presence of ceria allows an exchange of the oxygen species at a lower temperature than on alumina, but at high temperature the alumina imposes its mechanism of exchange.

4.1.2. Temperature Range and Number of Oxygen Species Exchanged during TPIE. The variations with the temperature of the rate of exchange and of the number of oxygen species exchanged are shown respectively in Figures 13 and 14. Table 2 gives the principal results of these measurements.

Each oxide studied presents a specific temperature range of oxygen exchange. Except for ceria and ceria-alumina that exchange following both simple and multiple exchange mechanisms, all the others follow the simple exchange mechanism (see section 4.1.2.) in which the first step is the dissociative adsorption of molecular oxygen at the oxide surface with formation of a triatomic intermediates.[34−36] From this point of view, it is not surprising that, after ceria, zirconia is the most active oxide for oxygen exchange. The presence, after a vacuum thermal treatment, of coordinatively unsatured Zr^{3+} centers at the surface of monoclinic zirconia, very resistant to the oxidation by molecular oxygen,[49] is a favorable factor to the dissociative adsorption of molecular oxygen. Silica oxygen species exchange at very high temperature, which agree with the zero activity of silica at 650 °C for oxygen exchange observed by Winter.[13]

On all the oxides, the number of oxygen atoms exchanged (see Figure 14) is greater than the number of oxygen surface species (10−15 at·nm^{-2}). During TPIE experiments, surface species and part of the bulk oxygen species are exchanged without any change observed in the mechanism (no change in the variation of the isotopomers partial pressures). For certain oxides (CeO_2-Al_2O_3, ZrO_2, MgO, and Al_2O_3) a constant rate of exchange with the temperature is noticed when an amount of oxygen corresponding to the number of surface species is exchanged (Figure 13).

4.2. Isotopic Exchange on Metal Supported Catalysts. 4.2.1 Activation of Oxygen Exchange by Noble Metals. 4.2.1-a. Presence of Rhodium. TPIE experiments of oxygen were carried out on alumina and rhodium-alumina supported catalysts (Figure 15). The presence of metal lowers the threshold of exchange temperature to 300 °C, the maximum rate is observed at 250 °C, instead of 620 °C for alumina by itself. At 300 °C, on rhodium-alumina sample, 10 at·nm^{-2} are exchanged, which corresponds to the number of the oxygen surface species.[50] The constant rate of exchange observed between 300 and 800 °C corresponds to the slow exchange of bulk oxygen of alumina. The principal effect of the presence of rhodium is to decrease the temperature range of surface oxygen species exchange: 200−300 °C for RhAl and 450−720 °C for Al_2O_3 alone.

4.2.1-b. Effect of Rhodium Particle Size. As the metal particle size contributes to the estimation of the surface diffusion coefficient (see eq 10), we study first the effect of the particle sizes on TPIE. Two samples of Rh/Al_2O_3 catalyst with the same amount of rhodium (0.5% wt.) but with two different average particle sizes (10 Å for RhAl-10 and 21 Å for RhAl-21) were tested in TPIE (Figure 16). When the average particle size is doubled, the threshold of the exchange temperature and the temperature of the maximum rate increase by 50 °C. It is to be noted that increase in the metal particle size has no effect on the amount of surface species exchanged, but only retards this exchange at high temperature (175−300 °C for RhAl-10 and 220−360 °C for RhAl-21) and decreases the value of the maximum rate of exchange. Once all the surface species are exchanged (≈10 at·nm^{-2} at 300 °C for RhAl-10 and at 360 °C for RhAl-21), no effect of particle size is noticeable with bulk oxygen exchange. The rates of bulk oxygen exchange are the same (≈15 × 10^{-4} at·nm^{-2} s^{-1}) for both catalysts.

The increase of metal particle size with a constant amount of metal loading leads to a decrease of the number of metal atoms accessible and of the total perimeter of metallic particles. The rate of the adsorption-transfer step of atomic oxygen species to oxide surface is then limited.

4.2.2. Mechanism of Exchange on Metal Supported Catalysts. As described in section 4.2.1, the metal particles on oxide surface increase considerably the oxygen exchange rate particularly at low temperatures. On metal supported catalysts, isotopic exchange mechanism occurs as shown in Figure 17. The equation of the exchange reaction could be written as 15

$$^{18}O^{18}O_{(gas)} + {}^{16}O_{(sup.)} \rightleftharpoons {}^{18}O^{16}O_{(gas)} + {}^{18}O_{(sup.)} \quad (15)$$

TABLE 2: Results of TPIE Experiments on Oxides

oxide	exchange temp range (°C)	temp of max. rate (°C)	R_e max. (10^{-4} at·nm^{-2} s^{-1})	E_a (kJ·mol^{-1})	Ne final (at nm^{-2})	exchange mechanism S for simple M for multiple
SiO_2	650 − >900	850	68	111	22.7	S
γ-Al_2O_3	460 − >800	620	62	125	27.5	S
ZrO_2	380−780	530	105	111	48.1	S
MgO	390 − >800	490	65	166	31.4	S
CeO_2	310−480	410	176	110	37.7	S and M
CeO_2-Al_2O_3	370 − >800	480	73	101	27.7	S and M

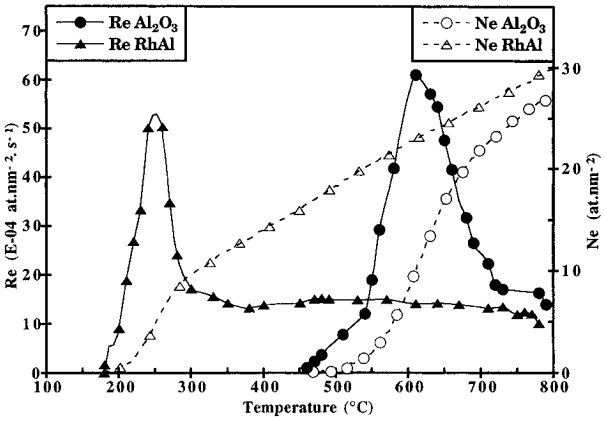

Figure 15. Influence of rhodium on TPIE of oxygen on alumina.

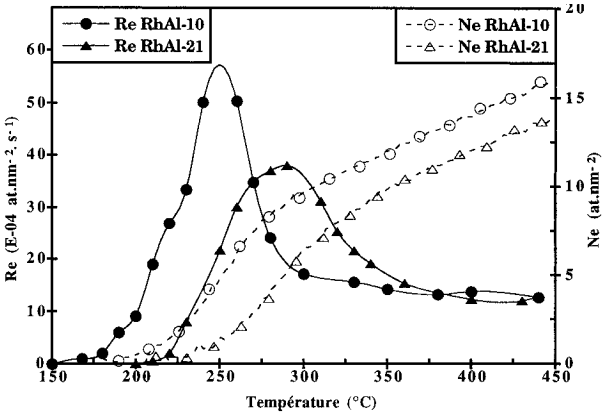

Figure 16. Effect of rhodium particle size.

The following steps are involved in this reaction: **1** - a dissociative adsorption of $^{18}O_2$ gas phase molecular on metal particles, **2** - a transfer of ^{18}O species from metal to oxide surface (spillover step), **3** - a surface migration of ^{18}O atomic species on the oxide surface to the sites of exchange, **4** - an exchange between ^{18}O species and ^{16}O species of the oxide surface, and **5** - ^{16}O species exchanged follow the reverse steps towards the metal particles and desorb as different isotopomers of molecular oxygen ($^{18}O^{16}O$ and $^{16}O^{16}O$).

To obtain measurements of surface mobility from this model, the three following conditions must be fulfilled.

a - The exchange must occur via metal particles. The rate of direct exchange between the gas phase and the oxide surface (step 6 in Figure 17) must be negligible. We check this by comparing the rate of exchange on oxide and on metal supported catalysts (see Table 3). On all oxides, excepted ceria and ceria-alumina, the rates of direct exchange between the gas phase and the oxide surface are negligible compared to the rate through rhodium particles at 400 °C.

b - The surface migration of oxygen species (step 3) must be the rate determining step of the mechanism. We check this by comparing the activation energies of isotopic exchange and of isotopic equilibration reactions. Figure 18 shows the Arrhenius curves of the rates of exchange (straight line) and equilibration (dotted line) on two supported zirconia catalysts.

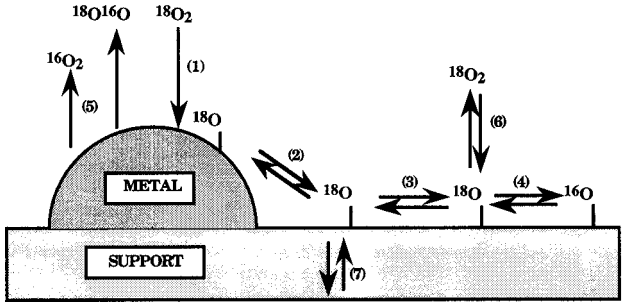

Figure 17. Oxygen exchange on rhodium catalysts.

TABLE 3: Comparison between the Rates of Exchange at T (°C) on the Oxides and on the Metal Supported Catalysts

oxide	T (°C)	R_e Rh/oxide / R_e oxide
SiO_2	450	∞
Al_2O_3	450	170
ZrO_2	450	260
MgO	400	260
CeO_2	400	40
CeO_2-Al_2O_3	450	69

TABLE 4: Comparison between the Activation Energies of the Heteroexchange and the Homoexchange

catalysts	temp range (°C)	E_a for heteroexchange (kJ·mol^{-1})	E_a for homoexchange (kJ·mol^{-1})
RhZr	$265 < T < 320$	80	84
	$320 < T < 450$	19	84
PtZr	$275 < T < 450$	37	39

TABLE 5: Temperature (T_o) of the Change in the Activation Energy of Exchange and the Activation Energies for the Rate of Exchange

catalysts	T_o (°C)	E_a(kJ·mol^{-1}) at $T > T_o$	E_a (kJ·mol^{-1}) at $T < T_o$
RhSi	330	42	53
RhAl	285	27	126
RhZr	280	19	80
RhMg	230	39	105
RhCe	350	30	64
RhCeAl	285	23	162

In the case of rhodium catalyst, the curve of exchange rate shows a change in the energy of activation in the region T_o = 200−350 °C. Taking into account the activation energy obtained at $T < T_o$ (E_a = 80 kJ·mol^{-1}) which is in the same order of those observed for the equilibration reaction (E_a = 84 kJ·mol^{-1}), the reasons for this change are as follows: (i) at $T < T_o$, the limiting step of exchange is the adsorption−desorption of oxygen on the rhodium particles (steps 1 and 5) and (ii) at $T > T_o$, the rate of exchange is determined by the oxygen mobility on the support (steps 2 and 3); in (ii) the apparent activation energy (Table 5) is lower than in (i).

In the case of platinum catalyst, no change can be observed and within the entire temperature range the activation energy

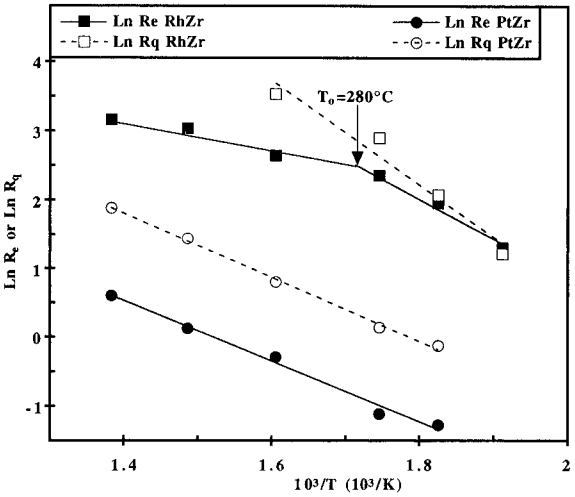

Figure 18. Arrhenius plots of the initial rates of exchange (straight line) and equilibration (dotted line) reactions on Rh and Pt zirconia supported catalysts.

TABLE 6: Surface Oxygen Coefficients Diffusion at 400 °C and Activation Energy of Diffusion

catalysts	D_s (10^{-19} $m^2 \cdot s^{-1}$)	E_a ($kJ \cdot mol^{-1}$)
RhCe	5700	49
RhMg	101	40
RhZr	57	90
RhCeAl	37	41
RhAl	20	20
RhSi	0.3	81

of exchange is the same as the one of equilibration (see Figure 18 and Table 4). Clearly in this case, the step of adsorption−desorption of oxygen on platinum particles is the rate determining step of the exchange mechanism. With platinum supported catalysts therefore we are not able to measure the oxygen mobility with isotopic exchange experiments.

For measuring oxygen surface mobility, rhodium is the best metal, but the exchange experiments must be carried above T_o. The values of T_o obtained for the various rhodium catalysts and the activation energies of exchange reaction at $T > T_o$ and at $T < T_o$ are listed in Table 5. The variations observed in the activation energies for $T < T_o$ show that the rate of oxygen adsorption on supported rhodium particles depend on the nature of the carrier.[51]

In absence of any analysis of ^{18}O concentration in the vicinity of metal particles, it is not easy to determine which step controls the rate of exchange: oxygen transfer (step 2) or oxygen diffusion (step 3). In the case of hydrogen, it has been shown by Cevallos-Candau and Conner[52] that spillover was the rate controlling step for hydrogen exchange on Pt/SiO_2. Theoretical calculations made with MgO as a support seem to demonstrate that oxygen transfer at the rhodium/support interface is energetically less demanding than the site-to-site migration on the support.[53] It can thus be assumed that surface diffusion is the rate controlling step for oxygen exchange.

c - The third and last condition concerns the difference between surface and bulk oxygen diffusion. Taking into account that surface oxygen mobility (step 3) is faster than bulk oxygen mobility (step 7), we could distinguish between these two processes by calculating the number of oxygen species exchanged for each time and by studying the shape of the curves representing these two diffusion processes (see Figure 9).

4.2.3. Surface and Bulk Diffusion Coefficients. 4.2.3-a. Surface Diffusion Coefficients. To fulfill all the previous conditions, we chose to carry out ISIE experiments between T_o and 400 °C (see Table 6).

TABLE 7: Bulk Oxygen Coefficients Diffusion at the Threshold Temperature of Bulk Diffusion

catalysts	T (°C)	D_r (10^{-23} $m^2 \cdot s^{-1}$)
RhCe	350	50
RhCeAl	300	11
RhZr	400	60
RhAl	450	7

TABLE 8: Results of CO_2 Chemisorption and Thermodesorption ($molec \cdot nm^{-2}$)

oxide	CO_2 chemisorbed before TPD	CO_2 thermodesorbed	CO_2 chemisorbed after TPD
SiO_2	0	0	0
γ-Al_2O_3	0.17	0.18	0.18
CeO_2-Al_2O_3	0.44	0.43	0.42
MgO	1.77	2.20	1.71
ZrO_2	1.45	1.52	1.82
CeO_2	3.23	3.05	3.01

From these results, three groups of oxides can be distinguished: **group A:** CeO_2 was the only oxide studied in this group. Its oxygen mobility was at least 60 times greater than that of the other oxides, **group B:** constituted by MgO, ZrO_2, CeO_2-Al_2O_3, and Al_2O_3 with an average value of oxygen surface mobility, and **group C:** constituted by SiO_2 with a very low oxygen mobility.

It is to be remarked that the presence of rhodium particles on the oxide surface does not modify the properties of the oxygen in the oxide. The lower the temperatures of the oxygen exchange on the bare oxide (TPIE experiments Table 2), the greater the surface mobility on rhodium supported catalysts (ISIE experiments Table 6). The presence of ceria decreases the temperatures of exchange of alumina and increases the surface mobility on RhCeAl.

4.2.3-b. Bulk Diffusion Coefficients. On oxides with a large oxygen surface mobility (CeO_2, ZrO_2, CeO_2-Al_2O_3, and Al_2O_3) we noticed for temperatures between 300 and 450 °C a bulk oxygen mobility (see Table 7). Like for surface diffusion, bulk diffusion coefficients follow the variations of exchange rates on the bare oxides, except for MgO on which no bulk mobility was observed between 250 and 450 °C. The presence of ceria increases the oxygen bulk mobility in alumina; this bulk mobility is noticeable above 300 °C on the biphasic oxide and above 450 °C on alumina.

4.3. Oxide Basicity Measurements. As discussed in the introduction, CO_2 chemisorption at room temperature is used to determine oxide surface basicity. To obtain accurate measurements, we proceed in three steps as described in the experimental part: chemisorption, TPD between 25 and 500 °C followed by a second chemisorption at room temperature (see Table 8).

Before discussing these results, we must keep in mind that the adsorption of CO_2 leads to oxide surface species which depend on the nature of the basic sites.[22] When the adsorption occurs on a basic hydroxyl group, there is formation of a surface hydrogen carbonate species and when it is on a basic oxygen ion, different kinds of carbonate species could be formed, depending whether there is participation or not of neighboring metal ions.[19] When the adsorption occurs on a very basic surface oxide the formation of bulk carbonate species is possible.[19,54,55]

There is a good coherence between the amounts of CO_2 chemisorbed and thermodesorbed (Table 8). These amounts allowed us to classify the oxides in three groups (Figure 19): **group I** is constituted only by SiO_2 on which no CO_2 chemisorption was observed, **group II** is constituted by Al_2O_3 and CeO_2-Al_2O_3 chemisorbing, respectively, 0.2 and 0.5 mol-

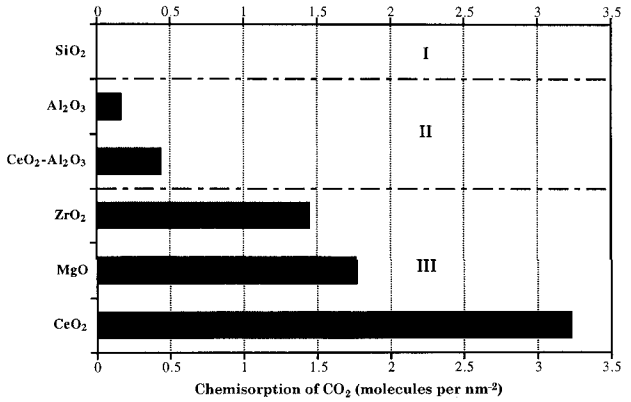

Figure 19. Chemisorption of CO_2 on the oxide surfaces at room temperature.

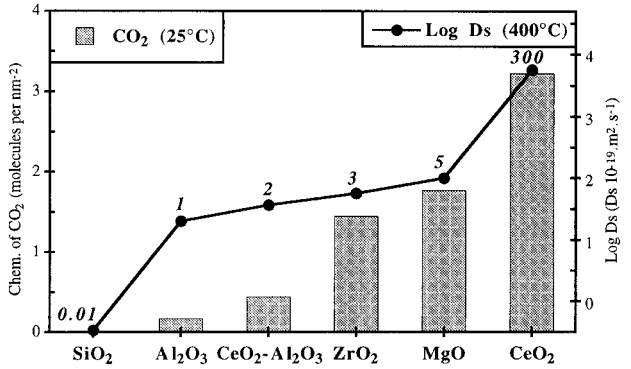

Figure 20. Correlation between oxygen surface mobility and oxide surface basicity.

ecule of CO_2 per nm^{-2}. These low values already observed by Mulcahy et al.,[56] show that on alumina only part of the hydroxyl group sites chemisorbed carbon dioxide. It must be noticed that the presence of a small amount of ceria (12% wt) doubles the amount of CO_2 chemisorbed on alumina, and **group III** is constituted by ZrO_2, MgO, and CeO_2 that chemisorbed over 1 molecule of CO_2 per nm^{-2}. These oxides have a relatively strong surface basicity.[22] The apparently greater basic surface for ceria than for magnesia could also be due to a reoxidation by CO_2 of partially reduced ceria sites associated with oxygen vacancies as previously mentioned by Lavalley.[19]

5. Discussion

Isotopic exchange carried out on oxides (TPIE) allows us to establish a scale of values for oxygen exchange versus temperature. A classification of oxygen mobility at 400 °C was made from the results (ISIE) obtained with Rh supported catalysts. The same oxide order can be observed for the scale of values obtained with the bare oxides and the classification obtained with Rh catalysts. There is obviously a correlation between oxygen mobilities and intrinsic oxide properties particularly their surface basicity and their metal−oxygen bond strengths.

Surface basicities determined by carbon dioxide chemisorptions allow us to establish another classification based on oxide basicity (Figure 19). This classification agrees with previous works involving CO_2 chemisorption[20,22] or other probe molecule conversion.[57] A good correlation exists between oxygen mobility at 400 °C and CO_2 chemisorption at room temperature (Figure 20): oxygen mobility increases with oxide basicity. Yet, it seems that this oxygen mobility on alumina and on ceria alumina is great in comparison with their surface basicity. In the same way we attributed the large amount of CO_2 chemisorbed on ceria to the presence of oxygen vacancies, the correlation observed between the basicity and the oxygen

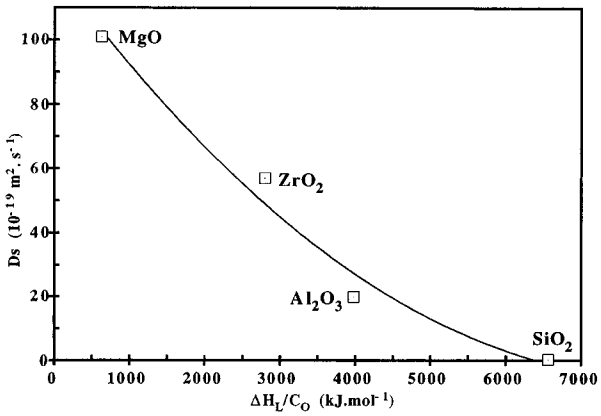

Figure 21. Correlation between the oxygen surface mobility and the strength of metal−oxygen bonds.

TABLE 9: Thermodynamic Values Used To Determine the Strength of Metal−Oxygen Bonds in the Supports

oxide	ΔH_L (kJ·mol^{-1})	C_o	$\Delta H_L/C_o$ (kJ·mol^{-1})
SiO_2	13125	2	6562
γ-Al_2O_3	15916	4	3979
MgO	3795	6	632
ZrO_2	11188	4	2797
CeO_2	9627	4	2407

mobility for this oxide suggests that the presence of oxygen vacancies also increases the oxygen mobility on ceria.

Because oxygen mobility requires at least a partial scission of the metal−oxygen bond in the supports, we were tempted to correlate oxygen surface diffusion coefficients with the strength of this metal−oxygen bond. This bond strength can be estimated from the value of the lattice energy ΔH_L given by the Born-Fajans-Haber cycle.[58] To obtain a good accuracy with the values of the lattice energy and the strength of the metal−oxygen bond, we must take into account the coordination value of oxygen (C_o) in each lattice: the values of ΔH_L considered[58] are therefore divided by C_o. All these data appear in Table 9; the values of C_o are determined according to the structures of the different oxides described in section 2.1. Figure 21 gives the correlation between the strengths of the metal−oxygen bond and the values of oxygen diffusion at 400 °C. Except for ceria (which is not represented in Figure 21), oxygen mobility increases when the strength of the metal−oxygen bond decreases. Although the strength of the metal−oxygen bond for ceria is between the strengths of the metal−oxygen bond of alumina and of zirconia (Table 9), the value of oxygen diffusion on ceria is 300 times higher than on alumina. This fact, correlated with the high amount of CO_2 chemisorbed on CeO_2, confirms that it is largely due to the presence of oxygen vacancies on this oxide.

6. Conclusion

The following conclusions can be drawn from the present study.

(**a**) TPIE of oxygen carried out at oxide surfaces allows determination of both the temperature range and the mechanism of oxygen isotopic exchange. Each oxide exchanges oxygen in the following order of temperature (first figure: temperature of the beginning of exchange; second figure: temperature of the maximal rate of exchange):

$$CeO_2\ (310\ °C;\ 410\ °C) \gg CeO_2\text{-}Al_2O_3\ (370\ °C;\ 480\ °C) \approx MgO\ (390\ °C;\ 490\ °C) > ZrO_2\ (380\ °C;\ 530\ °C) \gg Al_2O_3\ (460\ °C;\ 620\ °C) \gg SiO_2\ (650\ °C;\ 850\ °C)$$

On ceria, both simple and multiple exchange mechanisms occur in the same proportion whatever the temperature. From the very beginning of the reaction, the presence of multiple exchange would be due to the existence of diatomic oxygen species at the ceria surface.

The presence of ceria (12% wt) supported on alumina surface decreases the threshold exchange temperature of alumina by about 100 °C. Moreover in the temperature range where alumina alone is inactive, the exchange occurs according to a simple and a multiple mechanism as on ceria but involves a greater amount of oxygen than on ceria. There are strong interactions between ceria and alumina at the surface of this ceria modified alumina even if no mixed oxide structure has been detected by XRD measurements.

(**b**) The presence of rhodium supported at the oxide surface allows one to determine the surface and the bulk oxygen mobility between 300 and 400 °C. At 400 °C, the relative oxygen surface diffusion coefficients decrease in the following order (base 100 for alumina):

$$CeO_2\ (28\ 100) \gg MgO\ (500) > ZrO_2\ (280) > CeO_2\text{-}Al_2O_3\ (180) > Al_2O_3\ (100) \gg SiO_2\ (1.7)$$

A first significant fact is that the classification of the oxides is practically the same for both oxygen exchange on bare oxides and surface oxygen mobility on rhodium catalysts.

(**c**) For CeO_2, CeO_2-Al_2O_3, Al_2O_3, and ZrO_2, bulk oxygen diffusion occurs between 300 and 450 °C. The major fact is the promotion of this diffusion within the alumina network by the presence of ceria at the alumina surface. On alumina alone, bulk oxygen diffusion is only observed at 450 °C but on ceria-alumina biphasic oxide, bulk oxygen diffusion in alumina starts at 300 °C with a higher oxygen bulk diffusion coefficient. Compared to alumina, zirconia shows a very great internal mobility of oxygen.

(**d**) The rate of oxygen surface diffusion increases when the oxide surface basicity increases and when the strength of the metal−oxygen bond decreases. The presence of oxygen vacancies at the surface of ceria increases the oxygen surface diffusion and the carbon dioxide chemisorption without there being any correlation with the normal strength of the Ce−O bond.

References and Notes

(1) Duprez, D. *Appl. Catal.* **1992**, *82*, 111.
(2) Grenoble, D. C. *J. Catal.* **1978**, *51*, 212.
(3) Duprez, D.; Pereira, P.; Miloudi, A.; Maurel, R. *J. Catal.* **1978**, *75*, 151.
(4) Yao, H. C.; Yu Yao, Y. F. *J. Catal.* **1984**, *86*, 254.
(5) Weng, L. T.; Delmon, B. *Appl. Catal.* **1992**, *81*, 141.
(6) Sermon, P. A.; Bond, G. C. *Catal. Rev.* **1973**, *8*, 211.
(7) Conner, W. C. Jr.; Pajonk, G. M.; Teichner, S. J. *Adv. Catal.*, **1986**, *34*, 1.
(8) *Spillover of Adsorbed Species*, Pajonk, G. M., Teichner, S. J., Germain, J. E., Eds.; Proc. 1st Int. Conf. Spillover, Lyon-Villeurbanne, Stud. Surf. Sci. Catal., Vol. 17; Elsevier: Amsterdam, 1983.
(9) Proc. *2nd Int. Conf. on Spillover*; Steinberg, K. H., Ed.; K. Marx Universitat: Leipzig, 1989.
(10) *New Aspects of Spillover Effect in Catalysis*; Inui, T., Fujimoto, K., Uchijima, T., Masai, M., Eds.; Proc. 3rd Int. Conf. on Spillover, Kyoto, Stud. Surf. Sci. Catal., Vol. 77, Elsevier: Amsterdam, 1993.
(11) Conner, W. C.; Falconer, J. L. *Chem. Rev.* **1995**, *95*, 759.
(12) Winter, E. R. S. *Adv. Catal.* **1958**, *10*, 196.
(13) Winter, E. R. S. *J. Chem. Soc.* **1968**, *1*, 2889.
(14) Boreskov, G. K. *Adv. Catal.* **1964**, *15*, 285.
(15) Boreskov, G. K.; Muzykantov, V. S. *Ann. New York Acad. Sci.* **1973**, *213*, 137.
(16) Novakova, J. *Catal. Rev.* **1970**, *4*, 77.
(17) Klier, K.; Novakova, J.; Jiru, P. *J. Catal.* **1963**, *2*, 479.
(18) Abderrahim, H.; Duprez, D. In *Proc. 1st Int. Symp. Catalysis and Automotive Pollution Control (CAPOC 1)*, Crucq, A., Frennet, A., Eds.; Brussels, 1986, Stud. Surf. Sci. Catal., Elsevier: Amsterdam, 1987; Vol. 30, p 359.
(19) Lavalley, J. C. *Trends Phys. Chem.* **1991**, *2*, 305.
(20) Rethwisch, D. G.; Dumesic, J. A. *Langmuir* **1986**, *2*−1, 73.
(21) Zhang, G.; Hattori, H.; Tanabe, K. *Appl. Catal.* **1988**, *36*, 189.
(22) Auroux, A.; Gervasini, A. *J. Phys. Chem.* **1990**, *94*, 6371.
(23) Beck, D. D.; Capehart, T. W.; Hoffman, R. W. *Chem. Phys. Lett.* **1989**, *159*, 207.
(24) Haneda, M.; Miki, T.; Mizushima, T.; Kakuta, N.; Ueno, A. Proc. *10th Int. Congr. Catal., Budapest, 1992*, Guczi, L., Solymosi, F., Tetenyi, T., Eds.; New Frontiers in Catalysis: Elsevier Science Publishers: Vol. C, p 2079.
(25) Shyu, J. Z.; Otto, K. *J. Catal.* **1989**, *115*, 16.
(26) Moroz, E. M.; Drozdov, W. A.; Ushakov, V. A.; Dzhunusov, A. K.; Tsyrulnikov, P.-G. *React. Kin. Catal. Lett.* **1990**, *41*, 109.
(27) Lange, F. F. Jr. *Mater. Sci.* **1982**, *17*, 225.
(28) Mercera, P. D. L.; Van Ommen, J. G.; Doesburg, E. B. M.; Burggraaf, A. J.; Ross, J. R. H. *Appl. Catal.* **1990**, *57*, 127.
(29) Mc Cullough, J. B.; Trueblood, K. M. *Acta Crystallogr.* **1959**, *12*, 507.
(30) Smith, D. K.; Newkirk, H. W. *Acta. Cryst.* **1965**, *18*, 983.
(31) Abderrahim, H.; Duprez, D. Proc. *9th Int. Congr. Catal., Calgary, 1988*, Philipps, M. J., Terman, M., Eds.; Chemical Institute Canada: Ottawa, Canada, Vol. 3, p 1246.
(32) Duprez, D. *J. Chim. Phys.* **1983**, *80 n*° 6 , 487.
(33) Laachir, A.; Perrichon, V.; Badri, A.; Lamotte, J.; Catherine, E.; Lavalley, J. C.; El Fallah, J.; Hilaire, L.; Le Normand, F.; Quemere, E.; Sauvion, G. N.; Touret, O. *J. Chem. Soc., Faraday Trans.* **1991**, *87*, 1601.
(34) Bielanski, A.; Haber, J. *Catal. Rev.* **1979**, *19*, 1.
(35) Che, M.; Tench, J. *Adv. Catal.* **1982**, *31*, 7.
(36) Che, M.; Tench, J. *Adv. Catal.* **1983**, *32*, 1.
(37) Meriaudeau, P.; Vedrine, J. C. *J. Chem. Soc., Faraday Trans. 1* **1976**, *72*, 472.
(38) Cunningham, J.; Goold, E. L.; Fierro, J. L. G. *J. Chem. Soc., Faraday Trans. 1* **1982**, *78*, 785.
(39) Duprez, D.; Abderrahim, H.; Kacimi, S.; Riviere, J. In *2nd Int. Conf. on Spillover*; Steinberg, K. H., Ed.; K. Marx Universitat: Leipzig, 1989; p 127.
(40) Kramer, R.; Andre, M. *J. Catal.* **1979**, *58*, 287.
(41) Cavanagh, R. R.; Yates Jr., J. T. *J. Catal.* **1981**, *68*, 22.
(42) Duprez, D.; Miloudi, A. In *Spillover of Adsorbed Species*; Pajonk, G. M., Teichner, S. J., Germain, J. E., Eds.; Elsevier: Amsterdam, 1983; p 163.
(43) Kakioka, H.; Ducarme, V.; Teichner, S. J. *J. Chim.Phys.* **1971**, *n*° 11−12, 1715.
(44) Cunningham, J.; Cullinane, D.; Farrell, F.; O'Driscoll, J. P.; Morris, M. A. *J. Mater. Chem.* **1995**, *5(7)*, 1027.
(45) Gideoni, M.; Steinberg, M. *J. Solid State Chem.* **1972**, *4*, 370.
(46) Che, M.; Kibblewhite, J. F. J.; Tench, A. J.; Dufaux, M.; Naccache, C. *J. Chem. Soc., Faraday Trans. 1* **1973**, *69*, 857.
(47) Li, C.; Domen, K.; Maruya, K.; Onishi, T. *J. Am; Chem. Soc.* **1989**, *111*, 7683.
(48) Madier, Y.; Martin, D.; Duprez D. Unpublished results.
(49) Morterra, C.; Giamello, E.; Orio, L.; Volante, M. *J. Phys. Chem*, **1990**, *94*, 3111.
(50) Lippens, B. C.; Steggerda, J. J. In *Physical and Chemical Aspects of Adsorbents and Catalysts*; Linsen, B. H., Ed.; Academic Press: London, 1970; p 171.
(51) Martin, D.; Duprez, D. *Appl. Catal.* **1995**, *131*, 297.
(52) Cevallos-Candau, J. F.; Conner, W. C., Jr. *J. Catal.* **1987**, *106*, 378.
(53) Colin, M.; Pelissier, M. Unpublished results.
(54) Bernal, S.; Diaz, J. A.; Garcia, R.; Rodriguez-Izquierdo, J. M. *J. Mater. Sci.* **1985**, *20*, 537.
(55) Bernal, S.; Botana, F. J.; Garcia, R.; Rodriguez-Izquierdo, J. M. *React. Solids* **1987**, *4*, 23.
(56) Mulcahy, F. M.; Kozminski, K. D.; Slike J. M.; Ciccone, F.; Scierka, S. J.; Eberhardt, M. A.; Houalla, M.; Hercules, D. M. *J. Catal.* **1993**, *139*, 688.
(57) Gervasini, A.; Auroux, A. *J. Catal.* **1991**, *131*, 190.
(58) Lide, D. R. *CRC Hanbook of Chemistry and Physics*, 73rd ed.; CRC Press, Inc.: 1992−1993; pp 12−13 to 12−22.
(59) Isotopomers: two isotopomers of one molecule are two isomers in which isomerism is due only to the presence of different isotopes of the same element (for example $^{16}O^{16}O$ and $^{18}O^{16}O$ are two isotopomers of the O_2 molecule).

JP9531568